MULTIFRACTAL ANOMALY DETECTION IN IMAGES VIA SPACE-SCALE SURROGATES

Herwig Wendt, Lorena Leon, Jean-Yves Tourneret [*]

IRIT, Université de Toulouse, CNRS,
Toulouse INP, UT3, Toulouse, France.
name.surname@irit.fr

Patrice Abry

Univ Lyon, Ens de Lyon, Univ. Claude Bernard
CNRS, Laboratoire de Physique, Lyon, France
patrice.abry@ens-lyon.fr

ABSTRACT

Multifractal analysis provides a global description for the spatial fluctuations of the strengths of the pointwise regularity of image amplitudes. A global image characterization leads to robust estimation, but is blind to and corrupted by small regions in the image whose multifractality differs from that of the rest of the image. Prior detection of such zones with anomalous multifractality is thus crucial for relevant analysis, and their delineation of central interest in applications, yet has never been achieved so far. The goal of this work is to devise and study such a multifractal anomaly detection scheme. Our approach combines three original key ingredients: i) a recently proposed generic model for the statistics of the multiresolution coefficients used in multifractal estimation (wavelet leaders), ii) an original surrogate data generation procedure for simulating a hypothesized global multifractality and iii) a combination of multiple hypothesis tests to achieve pixel-wise detection. Numerical simulations using synthetic multifractal images show that our procedure is operational and leads to good multifractal anomaly detection results for a range of target sizes and parameter values of practical relevance.

***Index Terms*—** anomaly detection, multifractal analysis, surrogate data, wavelet leaders, log-cumulants

1. INTRODUCTION

Context. Multifractal analysis is a powerful theoretical and practical signal and image analysis that has found many successful applications of various natures in the past, see, e.g., [1] for examples. Its goal is to characterize the data under study based on the dynamics of its *pointwise regularity* h, usually defined as the Hölder exponent. The regularity fluctations are quantified globally, for the whole time series or image, by the so-called *multifractal spectrum* $\mathcal{D}(h)$, defined as the fractal (Hausdorff) dimensions of the iso-Hölder sets of the data, see, e.g., [1, 2] for details.

The practical estimation of $\mathcal{D}(h)$ relies on a so-called multifractal formalism, which provides a link between $\mathcal{D}(h)$ and the multi-scale statistics of multiresolution coefficients, such as wavelet or wavelet transform modulus maxima coefficients [3]. The state-of-the-art estimation procedure relies on coefficients specifically defined for multifractal analysis, the *wavelet leaders* [1, 2, 4–7]. Assuming that $\mathcal{D}(h)$ is the same throughout an image, the use of (space-averaged) empirical multiscale statistics leads to numerically robust estimation algorithms. However, such a global characterization makes the analysis blind to deviations of $\mathcal{D}(h)$ from its typical values in small regions, and is moreover corrupted by such anomalies.

Related work. The prior detection of multifractality anomalies is of great importance for the relevant interpretation of multifractality estimates in applications. In addition, their delineation is of great interest, e.g., in the context of medical imaging or remote sensing applications. However, this important problem has been addressed with limited success only, essentially formulated as a segmentation problem, see, e.g., [8–10]. One main difficulty is that it requires modeling the statistical fluctuations of multifractality estimates, which is a difficult task due to the involved statistical properties of multifractal images (non Gaussian images with strong dependencies across many length scales [11]). Another major difficulty stems from the paradox that characterizing pointwise regularity fluctuations practically requires studying their dynamics over several analysis scales, thus is inherently *non-local* (i.e., tied to space averages [1, 2, 12]) and hence antagonist to the goal of identifying and delineating (local) anomalies.

Goals and contributions. The goal of this work is to overcome the difficulties mentioned previously by designing, for the first time, a practically operational procedure for detecting pixels associated with abnormal multifractality in images. The method builds on the wavelet leader multifractal formalism, recalled in Sec. 2, yielding multifractality estiates for small patches centered at the image pixels, and is motivated by the statistical model for log-leaders of multifractal images proposed in [6, 7, 12]. Our main assumption is that anomalous regions are small in size and hence contribute little to the average multifractality of the image. Our key contributions, detailed in Sec. 3, are as follows. First, we propose an original space-scale surrogate data procedure in the log-wavelet

[*]Work supported by Grant ANR-18-CE45-0007 MUTATION.

leader domain that enables us to generate reference multifractality estimates for images with globally homogeneous multifractality, conditionally on the observed image. Second, we formulate a pixel-wise anomalous multifractality detector relying on a collection of surrogate estimates, false discovery rate correction for the multiple (pixel-wise) simultaneous detection problems, and majority vote over patches. Third, we study the performance of the proposed detector through a large set of numerical simulations with synthetic multifractal images with various anomaly sizes and strengths (cf., Sec. 4). Our results demonstrate the good performance of the detector and its applicability to real-world images. Sec. 5 concludes and points to future research directions.

2. MULTIFRACTAL ANALYSIS

Multifractal spectrum. Multifractal analysis quantifies the fluctuations in space of the pointwise regularity of a function $X(z) \in \mathbb{R}$, $z \in \mathbb{R}^2$ (image), where pointwise regularity is usually measured by the Hölder exponent $h(z) \geq 0$. The closer $h(z)$ to 0, the more irregular X around position z, see, e.g., [2] for details. The regularity fluctuations of X are then measured *globally* by the *multifractal spectrum*, defined as the collection of Hausdorff dimensions $\dim_H$ of the sets of points z at which $h(z)$ takes the value h [2],

$$\mathcal{D}(h) \triangleq \dim_H \{z : h(z) = h\}.$$

Wavelet leaders. 2D wavelets can be defined as tensorial products of the scaling function $\phi(x)$ and mother wavelet $\psi(x)$ of a 1D multiresolution analysis, $\psi^{(0)}(z) = \phi(z_1)\phi(z_2)$, $\psi^{(1)}(z) = \psi(z_1)\phi(z_2)$, $\psi^{(2)}(z) = \phi(z_1)\psi(z_2)$, $\psi^{(3)}(z) = \psi(z_1)\psi(z_2)$ [13, 14]. When ψ is suitably chosen, the dilated and translated templates denoted as $\psi^{(m)}_{j,\mathbf{k}}(z) = 2^{-j/2}\psi^{(m)}(2^{-j}z - \mathbf{k})$ $\psi^{(m)}$, where $a = 2^j$ and $z = 2^j\mathbf{k}$, $\mathbf{k} = (k_1, k_2)$, form a basis of $L^2(\mathbb{R}^2)$. The L^1 normalized discrete wavelet transform coefficients of an image X are defined as $d^{(m)}_X(j,k) = \langle \boldsymbol{X}, 2^{-j/2}\psi^{(m)}_{j,k}\rangle$, $m = 0, \ldots, 3$ [13]. Denote as $\lambda_{j,\mathbf{k}}$ the dyadic cube of side length 2^j centred at $\mathbf{k}2^j$ and $3\lambda_{j,\mathbf{k}} = \bigcup_{n_1,n_2=\{-1,0,1\}} \lambda_{j,k_1+n_1,k_2+n_2}$ the union with its eight neighbors. The wavelet leaders are defined as the supremum of the wavelet coefficients within $3\lambda_{j,\mathbf{k}}$ over all finer scales [2, 5], i.e.,

$$L(j,\mathbf{k}) \triangleq \sup_{m\in(1,2,3),\lambda'\subset 3\lambda_{j,\mathbf{k}}} |d^{(m)}_X(\lambda')|. \quad (1)$$

Multifractal formalism. Let $\ell(j,\mathbf{k}) \triangleq \ln L(j,\mathbf{k})$ denote the log-leaders of X. It can be shown [5] that the multifractal spectrum can be approximated as

$$\mathcal{D}(h) \approx 2 + \frac{c_2}{2}\left(\frac{h_1 - c_1}{c_2}\right)^2, \quad (2)$$

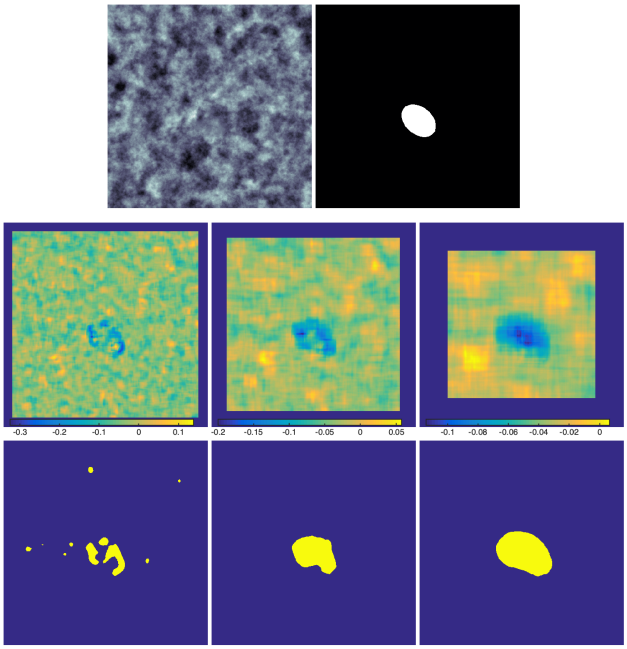

Fig. 1. Illustration for a single image. Top row: single realization of multifractal image (top left) and ground truth mask (right; black: $c_2 = -0.0001$, white: anomaly with $c_2 = -0.05$). Second row: Estimates $\hat{c}_2(z)$ obtained with patch sizes $P \in \{2^4, 2^5, 2^6\}$ (from left to right, respectively) Bottom row: corresponding detection results.

and that the coefficients c_1 and c_2 are directly related with the cumulants C_p of order p of $\ell(j,\mathbf{k})$ via the equation

$$C_p(j) = c^0_p + c_p \ln 2^j. \quad (3)$$

Relation (3) shows that the so-called *log-cumulants* c_p, and hence an estimate of $\mathcal{D}(h)$ using (2), can be computed by simple linear regressions across scale j. Below we only consider c_2, termed *multifractality parameter*, that quantifies the strength of multifractality of X (i.e., width of $\mathcal{D}(h)$).

3. MULTIFRACTAL ANOMALY DETECTION

3.1. Surrogate log-leaders

The properties of a multifractal image X are notoriously unfavorable for statistical processing since X is highly non Gaussian, strongly dependent and potentially non stationary [11]. Yet, it was shown in recent studies that the *log-leaders* $\ell(j,\mathbf{k})$ of an image X with homogeneous (i.e., constant throughout the image) multifractality can be well modeled by a multivariate Gaussian distribution, with a non-trivial and strong space-scale covariance that encodes the multifractality, see, e.g., [6, 7, 15]. Consequently, if the image contains a region with different homogeneous multifractalities, the log-leaders

associated with this region are also multivariate Gaussian, but with different parameters.

Time-scale surrogates. To detect a region of an image with abnormal multifractality, the method of surrogate data [16, 17], classically used to detect nonlinearities, is used to stationarize the multifractality of the image (similar to the approach in [18]) and thus to construct reference images with homogeneous multifractality throughout, i.e., without anomalous regions. Specifically, the procedure for each scale j is

1. remove the mean from $\ell(j,\cdot)$
2. compute the Fourier transform (FFT), $\hat{\ell}(j,\cdot)$ say
3. randomize the phase, yielding surrogates $\hat{\ell}^*(j,\cdot)$, where the same randomization is used for all scales to preserve the across-scale covariance of ℓ [19]
4. compute surrogate log-leaders $\ell^*(j,\cdot)$ by inverse FFT.

The so-obtained surrogate log-leaders ℓ^* are multivariate Gaussian with covariance concurring with homogeneous multifractality, regardless of whether X contains regions with anomalous multifractality or not. The procedure is repeated L times, yielding L independent copies of surrogates $\ell^{*(l)},\ l=1,\ldots,L$.

3.2. Anomalous multifractality detection

Test formulation. The problem of detecting whether the multifractality $c_2(z)$ associated with a pixel $X(z)$ of the image is anomalous or not can be formalized as testing the null hypothesis

$$H_0^{(z)} : c_2(z) = c_2^{ref}(z)$$

against the two-sided alternative $H_1^{(z)} : c_2(z) \neq c_2^{ref}(z)$, where $c_2^{ref}(z)$ is the multifractality that would be expected for a homogeneous image. To perform the test, we first compute multifractality estimates $\hat{c}_2(z)$ for each position z. To this end we evaluate (3) for the collection of log-leaders corresponding with a small patch $\mathcal{P}(z)$ of size $P\times P$ centered at z, denoted $\{\ell_\lambda\}_{\lambda\in\mathcal{P}(z)}$. Similarly, we compute surrogate multifractality estimates $\hat{c}_2^{*(l)}(z)$ for each set of surrogate leaders $\{\ell_\lambda^{*(l)}\}_{\lambda\in\mathcal{P}(z)},\ l=1,\ldots,L$, yielding a collection of surrogate multifractality estimates $\{\hat{c}_2^{*(l)}(z)\}_{l=1}^L$ for each pixel. By construction, the empirical distribution of $\hat{c}_2^*(z)$ yields an approximation for the distribution of $\hat{c}_2(z)$ under the null hypothesis and can therefore be used to perform the test. Let $0\le\gamma(z)\le 1$ denote the quantile of the distribution of $\hat{c}_2^*(z)$ that corresponds to the value of $\hat{c}_2(z)$, i.e.,

$$\gamma(z) \triangleq \frac{1}{L}\sum_{l=1}^{L}\delta(\hat{c}_2^{*(l)}(z)\le\hat{c}_2(z)),$$

where $\delta(\cdot)$ is the Kronecker delta. For some preset significance level α controlling Type I errors, the test then rejects $H_0^{(z)}$ if $\gamma(z)<\frac{\alpha}{2}$ and if $\gamma(z)>1-\frac{\alpha}{2}$, and the p-value for $H_0^{(z)}$ is given by

$$p(z) = 2\cdot\max(\gamma(z),1-\gamma(z)).$$

Multiple hypothesis correction. For an image with K pixels, the detection problem comprises multiple simultaneous hypotheses (one for each pixel). In the case of multiple simultaneous hypotheses, it is preferable to use corrections that reduce the number of false positives, and we follow the false discovery rate correction strategy of Benjamini-Hochberg [20]. This leads to the following decision rule to reject $H_0^{(z)}$,

$$d(z) = \begin{cases} 1 & \text{if } p(z) < k(z)\,\frac{q}{K}, \\ 0 & \text{otherwise.} \end{cases} \tag{4}$$

where $k(z) = 1+\text{card}(z' : p(z')<p(z))$ and q is the false discovery rate, i.e., the rate of Type I errors. Finally, since each pixel is covered by $P\times P$ patches, we perform a majority vote among the P^2 decisions for these patches to yield the final anomaly detection decision for pixel z defined as

$$\bar{d}(z) = \text{round}\left(P^{-2}\sum\nolimits_{z'\in\mathcal{P}(z)} d(z)\right).$$

4. PERFORMANCE ASSESSMENT

Numerical experiments. The proposed multifractal anomaly detection procedure was applied to 2D multifractal random walks (MRWs) of size 512×512. MRWs are synthetic multifractal processes whose multifractal properties resemble those of Mandelbrot's log-normal cascades, with $\mathcal{D}(h) = 2+\frac{c_2}{2}\left(\frac{h_1-c_1}{c_2}\right)^2$ (see, e.g., [21]). Assuming that the area of the image is normalized to equal 1, we consider three sizes of anomalies of area $\Delta\in\{0.01, 0.02, 0.05\}$ times the image size. A typical realization is plotted in Fig. 1 (top row) together with the ground truth for the position of a multifractal anomaly in the image. To estimate $c_2(z)$, we use the standard linear regression based estimator (using (3) as in [4,5,22]) for patches of size $P\in\{2^4,2^5,2^6\}$, and we set $q=0.01$ in the correction for multiple hypotheses. The average performance is quantified for 100 independent realizations using true positive rate (TPR, detection probability) and false positive rate (FPR, probability of false alarm).

Illustration for a single image. The output of the multifractal anomaly detector for a single image is plotted in Fig. 1 (bottom row) for patch size $P\in\{2^4,2^5,2^6\}$, respectively (from left to right). It demonstrates that the proposed detector is operational for application to a single image, and yields satisfactory results: for all patch sizes, the anomalous zone is detected and overall well localized. In this example, the most satisfactory results are achieved with the two larger patch sizes, which better match the size of the anomaly.

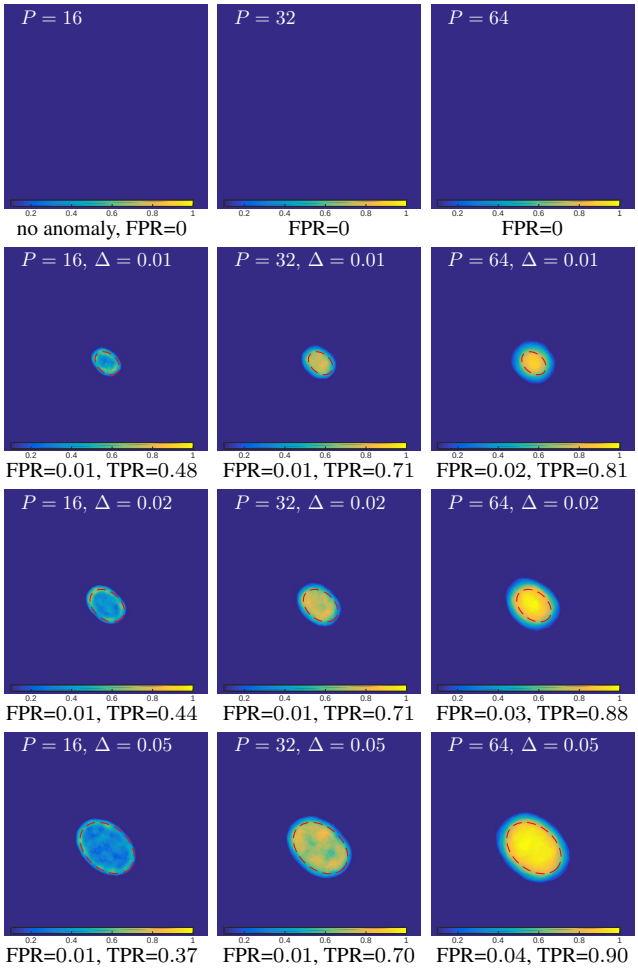

Fig. 2. Average detection probability ($c_2 = -0.0001$ vs. $c_2 = -0.05$). Top row: no anomaly. Rows 2 to 4: increasing target size (area Δ= 0.01, 0.02 and 0.05 of image size). From left to right: increasing patch size (16, 32 and 64 pixels).

Detection performance. Fig. 2 plots average detection results for 100 independent realizations when no anomaly is present (top row), and when an anomaly of increasing size $\Delta \in \{0.01, 0.02, 0.05\}$ is present (second to bottom row, respectively), for patch sizes 16, 32 and 64 (left to right column, respectively). It can be observed that in the absence of an anomaly in the image, the detector yields perfect results - indeed, the combination of correction for multiple hypotheses followed by majority vote makes a false positive unlikely. In the presence of anomalies, we correctly detect $40-90\%$ of the affected pixels, with only $1-4\%$ wrong detections. The highest detection rates for anomalous pixels are achieved with the largest considered patch size, yet at the price of slightly more false positives. These false positives are mostly located at the border of the anomaly, whose edges are "blurred". These observations for different patch sizes can be interpreted as a natural consequence of the bias-variance trade-off that is inherent to patch-based estimation.

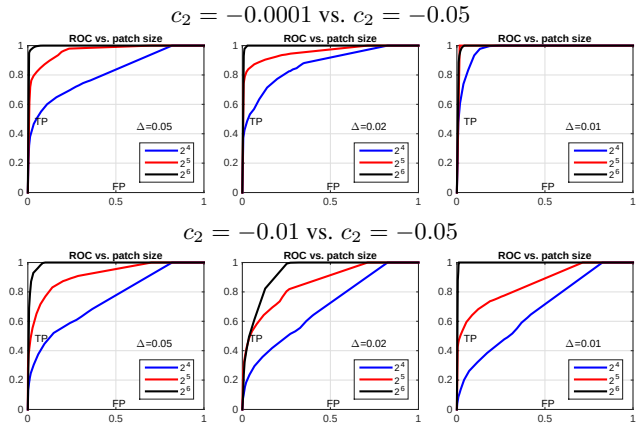

Fig. 3. **ROC curves.** From left to right: decreasing target size (area Δ= 0.05, 0.02, 0.01 of image size); $c_2 = -0.0001$ vs. $c_2 = -0.05$ (top row) and $c_2 = -0.01$ vs. $c_2 = -0.05$ (bottom row).

Fig. 3 presents a more quantitative analysis of the detection performance and plots receiver operator characteristic (ROC) curves for the three anomaly sizes and three patch sizes, and for two different scenarios of multifractality. It can be observed that the detection performance decreases when the difference between the values of c_2 inside and outside the abnormal region decreases. The results further confirm that the best overall detection performance is achieved with the largest considered patch size ($P = 2^6$), in which case the detection procedure is extremely accurate.

Overall, these results lead to conclude that the proposed multifractal anomaly detector is operational and yields satisfactory practical performance.

5. CONCLUSIONS

This work proposed a procedure that enables, for the first time, the detection of regions of anomalous multifractal properties in images. It makes use of a recently developed model for the multivariate statistics of log-leaders to simulate reference distributions for anomaly-free patch-wise multifractality estimates via an original surrogate data procedure. The surrogate empirical distributions of image patch multifractality are then used to estimate the probability that a patch in the image has a normal multifractality. These patch probabilities are finally combined into pixel-wise multifractal anomaly detections via Benjamini-Hochberg multiple decision corrections followed by majority vote. Numerical results with synthetic multifractal images demonstrate that the proposed procedure has good detection performance and can readily be applied for the analysis of real-world images. Future work will include applications to biomedical and remote sensing images, extensions to multifractal change detection for time series and to multivariate multifractal analysis.

6. REFERENCES

[1] S. Jaffard, P. Abry, and H. Wendt, "Irregularities and scaling in signal and image processing: Multifractal analysis," in *Benoit Mandelbrot: A Life in Many Dimensions*, Michael Frame, Ed. World scientific publishing, 2015.

[2] S. Jaffard, "Wavelet techniques in multifractal analysis," in *Fractal Geometry and Applications: A Jubilee of Benoît Mandelbrot, Proc. Symp. Pure Math.*, M. Lapidus and M. van Frankenhuijsen, Eds. 2004, vol. 72(2), pp. 91–152, AMS.

[3] P. Kestener, J. Lina, P. Saint-Jean, and A. Arneodo, "Wavelet-based multifractal formalism to assist in diagnosis in digitized mammograms," *Image Analysis and Stereology*, vol. 20, no. 3, pp. 169–175, 2001.

[4] H. Wendt, P. Abry, and S. Jaffard, "Bootstrap for empirical multifractal analysis," *IEEE Signal Process. Mag.*, vol. 24, no. 4, pp. 38–48, 2007.

[5] H. Wendt, S. G. Roux, S. Jaffard, and P. Abry, "Wavelet leaders and bootstrap for multifractal analysis of images," *Signal Process.*, vol. 89, no. 6, pp. 1100 – 1114, 2009.

[6] S. Combrexelle, H. Wendt, N. Dobigeon, J.-Y. Tourneret, S. McLaughlin, and P. Abry, "Bayesian estimation of the multifractality parameter for image texture using a Whittle approximation," *IEEE T. Image Proces.*, vol. 24, no. 8, pp. 2540–2551, 2015.

[7] H. Wendt, S. Combrexelle, Y. Altmann, J.-Y. Tourneret, S. McLaughlin, and P. Abry, "Multifractal analysis of multivariate images using gamma markov random field priors," *SIAM J. on Imaging Sciences (SIIMS)*, vol. 11, no. 2, pp. 1294–1316, 2018.

[8] T. Stojić, I. Reljin, and B. Reljin, "Adaptation of multifractal analysis to segmentation of microcalcifications in digital mammograms," *Physica A: Statistical Mechanics and its Applications*, vol. 367, pp. 494–508, 2006.

[9] A. Islam, K. M. Iftekharuddin, R. J. Ogg, F. H. Laningham, and B. Sivakumar, "Multifractal modeling, segmentation, prediction, and statistical validation of posterior fossa tumors," in *Medical Imaging 2008: Computer-Aided Diagnosis*. International Society for Optics and Photonics, 2008, vol. 6915, p. 69153C.

[10] D. Chakraborty, G. K. Sen, and S. Hazra, "High-resolution satellite image segmentation using hölder exponents," *Journal of Earth System Science*, vol. 118, no. 5, pp. 609, 2009.

[11] R. H. Riedi, "Multifractal processes," Tech. Rep., Rice Univ Houston Tx Dept Of Electrical And Computer Engineering, 1999.

[12] S. Combrexelle, H. Wendt, Y. Altmann, J.-Y. Tourneret, S. McLaughlin, and P. Abry, "Bayesian joint estimation of the multifractality parameter of image patches using gamma markov random field priors," in *Proc. IEEE Int. Conf. Image Proc. (ICIP)*, Phoenix, AZ, USA, September 2016.

[13] S. Mallat, *A Wavelet Tour of Signal Processing*, Academic Press, 3rd edition, 2008.

[14] J.-P. Antoine, R. Murenzi, P. Vandergheynst, and S. T. Ali, *Two-Dimensional Wavelets and their Relatives*, Cambridge University Press, 2004.

[15] L. Leon, H. Wendt, J.-Y. Tourneret, and P. Abry, "Bayesian estimation for the parameters of the bivariate multifractal spectrum," in *Proc. European Signal Processing Conference (EUSIPCO)*, Dublin, Ireland, August 2021.

[16] J. Theiler, S. Eubank, A. Longtin, B. Galdrikian, and J. D. Farmer, "Testing for nonlinearity in time series: the method of surrogate data," *Physica D: Nonlinear Phenomena*, vol. 58, no. 1-4, pp. 77–94, 1992.

[17] G. Lancaster, D. Iatsenko, A. Pidde, V. Ticcinelli, and A. Stefanovska, "Surrogate data for hypothesis testing of physical systems," *Physics Reports*, vol. 748, pp. 1–60, 2018.

[18] P. Borgnat, P. Flandrin, P. Honeine, C. Richard, and J. Xiao, "Testing stationarity with surrogates: A time-frequency approach," *IEEE Transactions on Signal Processing*, vol. 58, no. 7, pp. 3459–3470, 2010.

[19] D. Prichard and J. Theiler, "Generating surrogate data for time series with several simultaneously measured variables," *Physical review letters*, vol. 73, no. 7, pp. 951, 1994.

[20] Y. Benjamini and Y. Hochberg, "Controlling the false discovery rate: a practical and powerful approach to multiple testing," *Journal of the Royal statistical society: series B (Methodological)*, vol. 57, no. 1, pp. 289–300, 1995.

[21] R. Robert and V. Vargas, "Gaussian multiplicative chaos revisited," *Ann. Proba.*, vol. 38, no. 2, pp. 605–631, 2010.

[22] P. Abry, R. Baraniuk, P. Flandrin, R. Riedi, and D. Veitch, "Multiscale nature of network traffic," *IEEE Signal Proc. Mag.*, vol. 19, no. 3, pp. 28–46, 2002.